Characteristics of collectivity along the yrast line in even-even tungsten isotopes

Qiong Yang,[1] Hua-Lei Wang,[1,2,*] Min-Liang Liu,[3] and Fu-Rong Xu[4,5,6]
[1]*School of Physics and Engineering, Zhengzhou University, Zhengzhou 450001, China*
[2]*Henan Key Laboratory of Ion-beam Bioengineering (Zhengzhou University), Zhengzhou 450052, China*
[3]*Institute of Modern Physics, Chinese Academy of Sciences, Lanzhou 730000, China*
[4]*School of Physics, Peking University, Beijing 100871, China*
[5]*Institute of Theoretical Physics, Chinese Academy of Sciences, Beijing 100080, China*
[6]*Center of Theoretical Nuclear Physics, National Laboratory of Heavy Ion Collisions, Lanzhou 730000, China*
(Received 21 December 2015; published 5 August 2016)

The collective nature of high-spin yrast states in even-even $^{160-190}$W isotopes was systematically investigated by means of pairing self-consistent Woods-Saxon-Strutinsky calculations using the total Routhian surface approach in (β_2,γ,β_4) deformation space. The calculated ground-state deformations are consistent with previous calculations and available experimental data. The deformation energy curves are presented to show the shape and softness evolutions, in particular in the triaxial direction. The backbending or upbending behavior in moment of inertia is attributed to band crossing. It is found that the neutron rotation alignment is preferred for most of the W isotopes (e.g., in $^{164-180}$W), while in other nuclei the competition between the neutron and proton alignments may occur, even the proton alignment is favored in the very neutron-deficient nucleus ^{160}W. In addition, the evolution and transition between vibrational and rotational collective modes along the yrast line are investigated on the basis of the new centipedelike E-GOS (E-Gamma Over Spin) curves introduced by us, which to some extent explains the existing differences (e.g., in the moment of inertia) between theory and experiment.

DOI: 10.1103/PhysRevC.94.024310

I. INTRODUCTION

The spontaneous symmetry breaking mechanism implies that the nuclear mean-field approximation allows one to represent nuclei as deformed bodies in an intrinsic reference frame [1]. Deformed nuclei characterized by a nonspherical spatial distribution of nuclear density are known to exhibit the collective rotational motion, which will involve coherent contributions from many nucleons. That is, a deformed nucleus may rotate as a whole around an axis different from the nuclear symmetry axis (e.g., a collective rotation of a prolate nucleus around an axis perpendicular to the nuclear symmetry axis). Such phenomenon of nuclear rotation was discovered in the early 1950s following pioneering suggestions by Bohr and Mottelson [2]. As is known, the relation between the excitation energy E and spin I is usually smooth and obeys the $I(I+1)$ rule approximately. For a given angular momentum I, the lowest energy state $E(I)$ is called the yrast state and the sequence of all yrast states with increasing I is called the yrast line where the excited states are usually favorable to be populated, especially via the heavy-ion fusion-evaporation reaction. Some interesting phenomena such as the band crossing (backbending effect), yrast traps, and phase and shape transitions were found along the yrast line because the collective and noncollective modes of excitation may compete and/or combine in different ways [3,4].

In the mass region of $150 \leqslant A \leqslant 190$ (partly overlapping with the rare-earth region), nuclei exhibit a typical collective rotation with crossing bands. In the tungsten isotopic chain, thirty-five members from $^{158}W_{84}$ to $^{192}W_{118}$ (including five stable, seven neutron-rich, and 23 neutron-deficient isotopes and between $N = 82$ and 126 closed shell) have been discovered so far by using different reaction types such as heavy-ion fusion evaporation, light-particle reactions, neutron-capture reactions and projectile fragmentation [5]. However, according to, e.g., an extended Skyrme-Hartree-Fock-Bogoliubov mass model (HFB-14) [6] which is simultaneously fitted to masses and fission barriers, these tungsten isotopes ranging from $A = 154 - 250$ (97 nuclei) should be particle stable, showing there may be 62 nuclei to be discovered. It is also pointed out that eight additional nuclei beyond the proton drip line could live long enough to be measured [7]. Therefore, with the development of the radioactive beam facility, heavy-ion accelerator, and highly effective detector systems, there must be increasing interest in the structure evolution properties of these nuclei far from stability. For instance, very recently, a rotational-like ground-state band structure in the highly neuron-deficient nucleus ^{162}W was identified using the recoil-decay tagging method [8].

Theoretically, models for nuclear structure have been developed since the early days of nuclear physics about 80 years ago. They usually can be grouped into *ab initio* methods, self-consistent mean-field and shell model theories and macroscopic-microscopic methods [9]. It was found that the macroscopic-microscopic method has very high descriptive power. The root-mean-square deviation with respect to the 2353 known masses falls to 298 keV nowadays by using such method [10]. At present, even-even isotopes $^{160-190}$W have more than three yrast excited states (^{158,192}W only have one excited states), providing us a good opportunity to systematically investigate their high-spin properties. Therefore, we have performed the total Routhian surface (TRS) calculations, which is based on the macroscopic-microscopic model and

*wanghualei@zzu.edu.cn

cranking approximation [3], for even-even isotopes $^{160-190}$W, focusing on the band crossings, phase/shape transitions, nuclear softnesses and the reliability when extrapolating the model into the drip-line region. Note that such a cranking approximation introduced by Inglis [11,12] is one of the most common tools used for a microscopic description of nuclear rotations mainly because of its simplicity and semiclassical nature. It allows for a simultaneous description of collective and noncollective aspects of nuclear motion at high spins because their energy scales (frequencies) are of the same order of magnitude in nuclei. Therefore, the essential degree of freedom describing nuclear structure in the vicinity of the yrast line can be accounted for by the cranking model. We also performed the similar studies in Ba [13] and Os [14] isotopes recently, but only paying attention to the ground states.

The paper is organized as follows. We will outline the unified procedure of the TRS method and simultaneously provide the necessary references in Sec. II. The results and discussions are presented in Sec. III. Finally, we give a summary in Sec. IV.

II. THE MODEL

The pairing-deformation self-consistent TRS based on the macroscopic-microscopic model and cranked shell model (CSM) usually accounts well for the overall systematics of high-spin phenomena in rapidly rotating medium and heavy mass nuclei. Strictly speaking, the TRS calculations including pairing correlations were first introduced by Nazarewicz *et al.* [15] to describe the evolution of octupole deformation with rotational frequency in the Th-U region and further extended and used later for other mass regions by some authors (see, e.g., Refs. [16–18]). Nowadays, as one of the most powerful theoretical tools in the high-spin physics in nuclear structure, such an approach has several standard components, each one individually familiar from the literature. In the following, we will outline the unified procedure and simultaneously provide the necessary references.

First, by the Strutinsky method [19] generalized to the case of rotation [20–23], the total Routhian $E^{\omega}(Z,N,\hat{\beta})$ of a nucleus (Z, N) at frequency ω and deformation $\hat{\beta}$ (here one symbol stands for several shape degrees of freedom, e.g., β_2, γ, and β_4) can be obtained as [24],

$$E^{\omega}(Z,N,\hat{\beta}) = E^{\omega}_{\rm macr}(Z,N,\hat{\beta}) + \delta E^{\omega}_{\rm shell}(Z,N,\hat{\beta}) + \delta E^{\omega}_{\rm pair}(Z,N,\hat{\beta}), \quad (1)$$

where the first term on the right-hand side denotes the macroscopic (liquid drop) energy with the rigid-body moment of inertia calculated classically at a given deformation, assuming a uniform density distribution; $\delta E^{\omega}_{\rm shell}$ and $\delta E^{\omega}_{\rm pair}$, respectively, represent the single-particle shell correction and the pairing correction under rotation. After rearranging the right-hand side of Eq. (1) the total Routhian can be written as

$$E^{\omega}(Z,N,\hat{\beta}) = E^{\omega=0}(Z,N,\hat{\beta}) + [\langle \hat{H}^{\omega}(Z,N,\hat{\beta})\rangle - \langle \hat{H}^{\omega=0}(Z,N,\hat{\beta})\rangle] - \tfrac{1}{2}\omega^2[\mathcal{J}_{\rm macr}(A,\hat{\beta}) - \mathcal{J}_{\rm Stru}(Z,N,\hat{\beta})]. \quad (2)$$

The notations of the quantities in Eq. (2) are standard [16,24]. $E^{\omega=0}(Z,N,\hat{\beta})$ is the total energy at $\omega = 0$ (ground state) which consists of a macroscopic liquid-drop (LD) part $E_{\rm LD}(Z,N,\hat{\beta})$ (neglecting the superscript $\omega = 0$), a shell correction $\delta E_{\rm shell}(Z,N,\hat{\beta})$ and a pairing correction $\delta E_{\rm pair}(Z,N,\hat{\beta})$. The second term in the square brackets represents the energy change of the cranked HFB Hamiltonian $\hat{H}^{\omega}(Z,N,\hat{\beta})$ from rotation [16,24]. In the above equation, it is assumed that the average pairing energy of the liquid-drop term and the Strutinsky-smeared pairing energy cancel each other [24]. Therefore, one can further write Eq. (2) as [cf. Ref. [25] and references therein],

$$E^{\omega}(Z,N,\hat{\beta}) = E_{\rm LD}(Z,N,\hat{\beta}) + \delta E_{\rm shell}(Z,N,\hat{\beta}) + \delta E_{\rm pair}(Z,N,\hat{\beta}) + [\langle \hat{H}^{\omega}(Z,N,\hat{\beta})\rangle - \langle \hat{H}^{\omega=0}(Z,N,\hat{\beta})\rangle]. \quad (3)$$

So far, several phenomenological LD models with slightly different properties have been developed to be used for calculating the smoothly varying part, in which the dominating terms are mainly associated with the volume energy, the surface energy, and the Coulomb energy. In the present work, the macroscopic energy is obtained from the standard LD model with the parameters used by Myers and Swiatecki [26]. Because our attention is just on the energy surface, the nuclear potential energy relative to that of a spherical LD is adopted in the calculations [26,27]. Though such sharp-surface LD model does not consider the surface diffuseness, the surface curvature effect, and the finite range of the nuclear interaction, it provides a somewhat good description of nuclear ground-state properties and collective excitations. In Eq. (3), the shell correction $\delta E_{\rm shell}(Z,N,\hat{\beta})$ and the pairing correction $\delta E_{\rm pair}(Z,N,\hat{\beta})$ are calculated using the Strutinsky method [19] and Lipkin-Nogami (LN) method [28], respectively. The Strutinsky smoothing is performed with a sixth-order Laguerre polynomial and a smoothing range $\gamma = 1.20\hbar\omega_0$, where $\hbar\omega_0 = 41/A^{1/3}$ MeV. The LN method avoids the spurious pairing phase transition encountered in the simpler BCS calculation. Moreover, not only monopole but also doubly stretched quadrupole pairings are considered. The monopole pairing strength G is determined by the average gap method [29] and the quadrupole pairing strengths are obtained by restoring the Galilean invariance broken by the seniority pairing force [30]. The quadrupole pairing can affect rotational bandhead energies, moments of inertia, band-crossing frequencies, and signature inversion in odd-odd nuclei [31–34]. As shown in Eq. (3), the total energy will depend implicitly on the single-particle levels via the last three terms.

The single-particle levels are calculated by solving numerically the Schrödinger equation with the Woods-Saxon Hamiltonian [35],

$$H_{\rm WS} = T + V_{\rm cent}(\vec{r};\hat{\beta}) + V_{so}(\vec{r},\vec{p},\vec{s};\hat{\beta}) + \tfrac{1}{2}(1+\tau_3)V_{\rm Coul}(\vec{r},\hat{\beta}), \quad (4)$$

where the Coulomb potential $V_{\rm Coul}(\vec{r},\hat{\beta})$ defined as a classical electrostatic potential of a uniformly charged drop is added for protons. The central part of the WS potential which controls mainly the number of levels in the potential well is calculated

as

$$V_{\rm cent}(\vec{r},\hat{\beta}) = \frac{V_0[1 \pm \kappa(N-Z)/(N+Z)]}{1+\exp[{\rm dist}_\Sigma(\vec{r},\hat{\beta})/a]}, \quad (5)$$

where the plus and minus signs hold for protons and neutrons, respectively, and the a is the diffuseness of the nuclear surface. The term ${\rm dis}_\Sigma(\vec{r},\hat{\beta})$ denotes the distance of a point $\vec{r}$ from the nuclear surface Σ parametrized in terms of the multipole expansion of spherical harmonics $Y_{\lambda\mu}(\theta,\phi)$ (which are convenient to describe the geometrical symmetry), namely,

$$\Sigma : R(\theta,\phi) = r_0 A^{1/3} c(\hat{\beta}) \left[1 + \sum_\lambda \sum_{\mu=-\lambda}^{+\lambda} \alpha_{\lambda\mu} Y^*_{\lambda\mu}(\theta,\phi) \right], \quad (6)$$

where the function $c(\hat{\beta})$ ensures the conservation of the nuclear volume with a change in the nuclear shape and $\hat{\beta}$ denotes the set of all the deformation parameters. In general, a limiting value of $\lambda < A^{1/3}$ can be obtained by a crude estimate [36]. In the present shape parametrization, we consider quadrupole and hexadecapole degrees of freedom, including nonaxial deformations [that is, $\hat{\beta} \equiv (\alpha_{20},\alpha_{2\pm2},\alpha_{40},\alpha_{4\pm2},\alpha_{4\pm4})$]. Of course, the quantity $R(\theta,\phi)$ means the distance of any point on the nuclear surface from the origin of the coordinate system. Obviously, such parametrization will preserve three symmetry planes because only the even λ and even μ components are taken into account. After requesting the hexadecpole degrees of freedom to be functions of the scalars in the quadrupole tensor $\alpha_{2\mu}$, one can reduce the number of independent coefficients to three, namely, β_2, γ, and β_4, where

$$\begin{aligned}
\alpha_{20} &= \beta_2 \cos\gamma \\
\alpha_{22} &= \alpha_{2-2} = -\frac{1}{\sqrt{2}}\beta_2 \sin\gamma \\
\alpha_{40} &= -\frac{1}{6}\beta_4(5\cos^2\gamma + 1) \\
\alpha_{42} &= \alpha_{4-2} = -\frac{1}{12}\sqrt{30}\beta_4 \sin 2\gamma \\
\alpha_{44} &= \alpha_{4-4} = -\frac{1}{12}\sqrt{70}\beta_4 \sin^2\gamma.
\end{aligned} \quad (7)$$

Note that the (β_2,γ,β_4) parametrization has all the symmetry properties of Bohr's (β_2,γ) parametrization [2,37]. The spin-orbit potential which can strongly affect the level order is defined by

$$\begin{aligned}
&V_{so}(\vec{r},\vec{p},\vec{s};\hat{\beta}) \\
&= -\lambda\left[\frac{\hbar}{2mc}\right]^2 \left\{ \nabla \frac{V_0[1 \pm \kappa(N-Z)/(N+Z)]}{1+\exp[{\rm dist}_{\Sigma_{so}}(\vec{r},\hat{\beta})/a_{so}]} \right\} \times \vec{p}\cdot\vec{s},
\end{aligned} \quad (8)$$

where λ denotes the strength parameter of the effective spin-orbit force acting on the individual nucleons. The new surface Σ_{so} is different from the one in Eq. (5) because of the different radius parameter. In this work, we use the universal Woods-Saxon parameter set (including the 12 constants determined the potential parametrization) of Ref. [27], which is Z and N independent and can give a good description of the single-particle states, at least in the medium and heavy mass regions [38]. These WS parameters, taken from Ref. [27], are

(a) Radius parameters: $r_0(p) = 1.275$ fm, $r_0(n) = 1.347$ fm, $r_{0-so}(p) = 1.320$ fm, $r_{0-so}(n) = 1.310$ fm.
(b) Central potential depth parameters: $V_0 = 49.6$ MeV, $\kappa = 0.86$.
(c) Spin-orbit potential strength constants: $\lambda(p) = 36.0$, $\lambda(n) = 35.0$.
(d) Diffuseness parameters: $a_0(p) = a_0(n) = a_{0-so}(p) = a_{0-so}(n) = 0.70$ fm.

During the diagonalization process of the WS Hamiltonian, the eigenfunctions of the axially deformed harmonic oscillator in the cylindrical coordinate system with the principal quantum number $N \leq 12$ and 14 have been used as a basis for protons and neutrons, respectively. The results with such a basis cutoff are sufficiently stable with respect to a possible enlargement of the basis. In the presence of pairing, the LN technique [16,28] is used, which aims to minimize the expectation value of the operator,

$$\mathcal{H} = H_{\rm WS} + H_{\rm pair} - \lambda_1 N - \lambda_2 N^2, \quad (9)$$

where $H_{\rm pair}$ indicates the pairing interactions including the monopole and quadrupole pairing forces [29,30,34]. In the pairing windows, dozens of single-particle levels, the respective states (e.g., half of the particle number Z or N) just below and above the Fermi energy, are included empirically for both protons and neutrons. The LN pairing energy can be given by [28,39]

$$E_{\rm LN} = \sum_k 2{v_k}^2 e_k - \frac{\Delta^2}{G} - G\sum_k {v_k}^4 + G\frac{N}{2} - 4\lambda_2 \sum_k {u_k}^2 {v_k}^2, \quad (10)$$

where ${v_k}^2$, e_k, Δ, and λ_2 represent the occupation probabilities, single-particle energies, pairing gap, and number-fluctuation constant, respectively.

In the present TRS calculations, we consider the one-dimensional cranking approximation in addition to the residual pairing interactions, which indicates that the nuclear system is constrained to rotate around a fixed axis (e.g., the x axis with the largest moment of inertia) at a given frequency ω. The cranking Hamiltonian has the form,

$$H^\omega = H_{\rm WS} + H_{\rm pair} - \omega j_x. \quad (11)$$

The resulting cranking LN equation takes the form of the well-known Hartree-Fock-Bogolyubov-like (HFB) equation which can be solved by using the HFB cranking (HFBC) method [40] (also see, e.g., Ref [3], for a detailed description). The HFB-like equations have the following form (see, e.g., Ref. [16] and references therein for more details):

$$\begin{aligned}
&\sum_{\beta>0}\{[(e_\alpha - \lambda)\delta_{\alpha\beta} - \omega(j_x)_{\alpha\beta} - G\rho^*_{\bar{\alpha}\bar{\beta}} + 4\lambda_2\rho_{\alpha\beta}] \\
&\quad \times U_{\beta k} - \Delta\delta_{\alpha\beta}V_{\bar{\beta}k}\} = E_k U_{\alpha k}, \\
&\sum_{\beta>0}\{[(e_\alpha - \lambda)\delta_{\alpha\beta} - \omega(j_x)_{\alpha\beta} - G\rho_{\alpha\beta} + 4\lambda_2\rho^*_{\bar{\alpha}\bar{\beta}}] \\
&\quad \times V_{\bar{\beta}k} + \Delta^*\delta_{\alpha\beta}U_{\beta k}\} = E_k V_{\bar{\alpha}k},
\end{aligned} \quad (12)$$

where $\Delta = G\sum_{\alpha>0}\kappa_{\alpha\bar{\alpha}}$, $\lambda = \lambda_1 + 2\lambda_2(N+1)$, and $E_k = \varepsilon_k - \lambda_2$. Further, ε_k is the quasiparticle energy and α ($\bar{\alpha}$) denote the states of signature $r = -i$ ($r = +i$), respectively. The matrices ρ and κ correspond to the density matrix and pairing tensor. While solving the HFBC equations, pairing is treated self-consistently at each frequency ω and each grid point in the selected deformation space (pairing self-consistency). Certainly, symmetries of the rotating potential are used to simplify the cranking equations. For instance, in the present reflection-symmetric case, both signature r, and intrinsic parity π are good quantum numbers. Until now, one can obtain the energy relative to the nonrotating ($\omega = 0$) state, as seen in the last term of Eq. (3). After the numerically calculated Routhians at fixed ω are interpolated using a cubic spline function between the lattice points, the equilibrium deformation can be determined by minimizing the calculated TRS (deformation self-consistency). In addition, the HFBC method also allows one to calculate approximately the total angular momentum as functions of the rotational frequency ω, from which some quantities such as the kinematic and dynamical moments of inertia, the aligned angular momenta including the proton and neutron components, etc., can also be derived. The total collective angular momentum is calculated as follows [16]:

$$I_x = \sum_{\alpha,\beta>0}\langle\beta|j_x|\alpha\rangle\rho_{\alpha\beta} + \sum_{\alpha,\beta>0}\langle\bar{\beta}|j_x|\bar{\alpha}\rangle\rho_{\bar{\alpha}\bar{\beta}}, \qquad (13)$$

where ρ is the density matrix based on the representation of signature basis denoted by α, β ($\bar{\alpha}$, $\bar{\beta}$ are for the opposite signatures).

III. RESULTS AND DISCUSSION

In nuclear structure research, some phenomenological or empirical laws are usually used to evaluate the nuclear properties. Several phenomenological quantities and their evolutions as increasing neutron number are presented in Fig. 1 for W isotopes. The systematics of the energy ratio, $R_{4/2} = E_{4_1^+}/E_{2_1^+}$, which is arguably the best indicator of changes in low-lying nuclear structure, can provide a test of the axial assumption. The energy ratio $R_{4/2}$ is 3.3 for a well-deformed axially symmetric rotor, 2.5 for γ-unstable vibrator, and 2.0 for spherical vibrator, which, respectively, correspond to $SU(3)$, $O(6)$, and $U(5)$ dynamic symmetries in the algebraic view of the interacting boson model (IBM) [43,44]. Further, the $R_{4/2}$ value is about 2.9 for the $X(5)$ symmetry (the critical point of spherical to deformed transition path) and 2.2 for the $E(5)$ symmetry (the critical point of spherical to γ-unstable vibrator path) [45]. From Fig. 1(a), one can see that near the $N = 104$ midshell the $R_{4/2}$ ratios reach the maximum value ~3.3, indicating the maximum collectivity (although it seems that the maximum $R_{4/2}$ value does not appear at the $N = 104$ nucleus which may be γ soft relatively). The $R_{4/2}$ ratio has a decreasing trend as the neutron number moves away from the $N = 104$ midshell. All the $R_{4/2}$ values are more than the critical value 1.82 in the Mallmann plot showing undoubtedly the onset of collective characteristics [43]. Moreover, nine members from N=98–114 have the $R_{4/2}$ ratios beyond the shape or phase transition point to quadrupole deformed nuclei, 3.0. This is favorable to present cranking investigation.

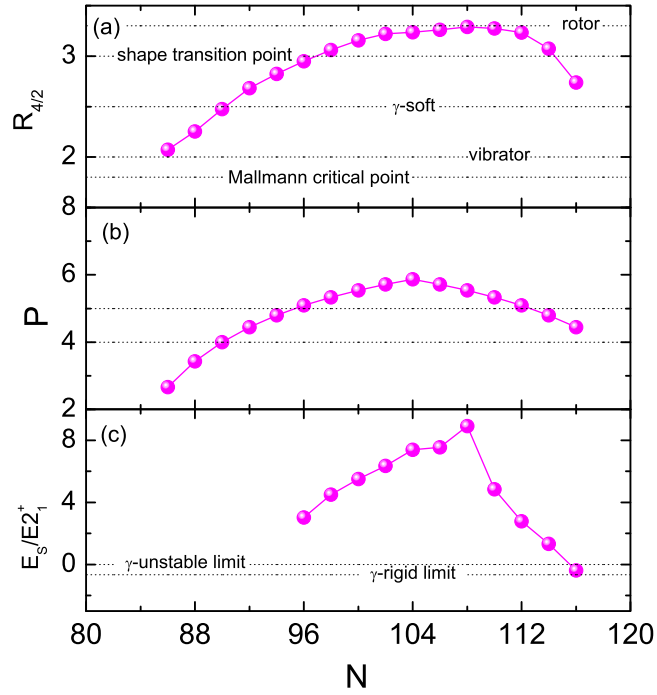

FIG. 1. The available phenomenological quantities $R_{4/2}$ ratio (a), P factor (b), and $E_S/E(2_1^+)$, $E_S = E(2_2^+) - E(4_1^+)$ (c) for even-even W isotopes as a function of the neutron number N. The dashed lines represent some corresponding critical points. See text for more details. The data are taken from Refs. [8,41,42].

Nuclear deformation may be explained as being from a competition between the pairing interaction of like nucleons and the neutron-proton interaction which is responsible for strong mixing of shell model configurations. The P factor [46–50] is another more sensitive phenomenological discovery related to nuclear collectivity and deformation, which is defined by

$$P \equiv \frac{N_p N_n}{N_p + N_n}, \qquad (14)$$

where N_p and N_n are the numbers of valence protons and neutrons, respectively; the product N_pN_n indicates the number of $p-n$ interactions and the summation $N_p + N_n$ denotes the number of pairing interactions. Obviously, this parameter can be viewed as the average number of interactions of each valence nucleon with those of the other type. It was pointed out by Casten *et al.* [47] that the transition to deformation generally occurs when $P \approx 4$–5, that is, each valence nucleon interacts with about 4–5 nucleons of the other type. Of course, it should be related to the relative integrated strengths of the $p-n$ and like-nucleon-pairing interactions. As shown in Fig. 1(b), all the P values are more than 4 except those of $^{160-164}$W, showing the onset of deformation in most of the nuclei. However, one can notice that the shape transition point ($R_{4/2} = 3.0$) corresponds to the critical point $P \approx 5$ rather than 4. Therefore, the $p-n$ and pairing interaction in this isotopic chain is worth investigating although it is beyond the scope of this work.

TABLE I. The calculated results (TRS) for ground-state equilibrium deformation parameters β_2 and β_4 for even-even $^{160-190}$W, together with the FY+FRDM (FF) [39], HFBCS [58], and ETFSI [59] calculations and partial experimental values (Expt.) [57] for comparison.

Nuclei	β_2					β_4			
	TRS[a]	FF	HFBCS	ETFSI	Expt.[b]	TRS	FF	HFBCS	ETFSI
^{160}W	0.122	0.089	0.00	0.14	—	0.013	0.003	0.00	0.00
^{162}W	0.148	0.134	0.14	0.17	—	0.011	0.015	−0.01	0.00
^{164}W	0.164	0.161	0.18	0.19	—	0.001	0.010	−0.01	0.00
^{166}W	0.176	0.181	0.18	0.21	—	−0.010	−0.004	−0.01	0.00
^{168}W	0.191	0.208	0.21	0.22	0.232	−0.016	0.000	−0.01	0.00
^{170}W	0.207	0.226	0.25	0.27	0.240	−0.012	−0.006	−0.01	0.00
^{172}W	0.230	0.254	0.23	0.29	0.284	−0.011	−0.001	−0.02	0.01
^{174}W	0.239	0.256	0.30	0.31	0.252	−0.018	−0.014	−0.02	0.00
^{176}W	0.243	0.266	0.30	0.31	—	−0.031	−0.032	−0.03	−0.02
^{178}W	0.241	0.267	0.33	0.31	—	−0.043	−0.048	−0.04	−0.02
^{180}W	0.238	0.258	0.26	0.27	0.255	−0.054	−0.067	−0.05	−0.05
^{182}W	0.234	0.259	0.24	0.27	0.251	−0.065	−0.084	−0.05	−0.05
^{184}W	0.227	0.240	0.24	0.25	0.236	−0.076	−0.095	−0.05	−0.07
^{186}W	0.217	0.230	0.21	0.25	0.228	−0.084	−0.107	−0.04	−0.06
^{188}W	0.200	0.212	−0.21	0.20	—	−0.082	−0.110	−0.05	−0.08
^{190}W	0.176	0.173	−0.20	0.19	—	−0.077	−0.097	−0.04	−0.06

[a]The calculated ground-state $|\gamma|$ values of $^{160-190}$W are always less than 2°.
[b]The uncertainties are less than 0.01 except for ^{172}W (0.014); see Ref. [57] for details.

The possible deviation from axial symmetry of the ellipsoidal nuclear shape, represented by the γ degree of freedom, will sensitively affect the so-called quasi-γ bandheads, namely, the second lowest 2^+ states of even-even nuclei in this mass region. The quantity $E_S/E(2_1^+)$ introduced by Watanabe *et al.* [51] usually can serve as a global signature of the structural evolution involving axial asymmetry, where E_S denotes the energy difference between the 2_2^+ and 4_1^+ states. As is known, the simplest symmetry limit model describing triaxiality of nuclei is the rigid triaxial rotor model of Davydov–Filippov [52] with the fixed deformation parameters β_2 and γ. In the case of the rigid-triaxial rotor with $25^\circ \leqslant \gamma \leqslant 30^\circ$, the 2_2^+ state will go under the 4_1^+ level and reach the bottom at the extreme of triaxiality with $\gamma = 30^\circ$ [At this time, the quantity $E_S/E(2_1^+)$ will reach the smallest value −0.67). The other symmetry limit model describing triaxiality is the Wilets-Jean model [53] of γ-unstable deformation, i.e., γ-independent collective potential. In the γ-independent limit (a flat potential at the γ direction) of the Wilets-Jean model, the value of $E_S/E(2_1^+)$ is zero because the 2_2^+ and 4_1^+ states are completely degenerate. The negative values of $E_S/E(2_1^+)$ between these two extremes 0 and −0.67 indicate likely γ-soft potentials with shallow minima at the average γ value close to 30°. The nucleus with a positive value of $E_S/E(2_1^+)$ will possess an axially symmetric shape. Indeed, the experimental energies of the $K^\pi = 2^+$ quasi-γ bands have been systematically identified in the tungsten, osmium, platinum, and mercury isotopes; cf. Refs. [42,54–56] and references therein. In Fig. 1(c), we show the available $E_S/E(2_1^+)$ ratios for the tungsten isotopes. It is found that all the values are larger than zero except for that of $^{190}W(\approx -0.38)$. In addition, one can see that the $N = 108$ nucleus ^{182}W owns the maximum $E_S/E(2_1^+)$ value, indicating a possible maximum stiffness in the triaxial direction. Moreover, the $E_S/E(2_1^+)$ ratio has a decreasing trend when N moves away from 108. These properties are basically in agreement with the following calculations.

Table I shows the calculated ground-state deformations β_2 and β_4, which are confronted with experiments and/or other accepted theories. Note that the experimental β_2 are deduced from the intrinsic quadrupole moment related to the reduced electric quadrupole transition probability $B(E2)$ [57]. Several other results are, respectively, based on the fold-Yukawa (FY) single-particle potential and the finite-range droplet model (FRDM) [39], the Hartree-Fock-BCS (HFBCS) [58], and the extended Thomas-Fermi plus Strutinsky integral (ETFSI) methods [59], which can be used to evaluate our TRS calculations. As is seen in this table, the predicted ground-state β_2, β_4 deformations are basically in agreement with the experimentally measured results although there is still a systematic underestimation for β_2. This is in agreement with the analysis by Dudek *et al.* [60] where a corrected formula is suggested to modify the shape inconsistency. All the theoretical results cannot completely agree with the data, but their trends are similar. As expected, the β_2 deformation reaches a maximum near $N = 104$ midshell nucleus ^{178}W (halfway between the $N = 82$ and $N = 126$ major shell closures) and decreases as the neutron number N moves away from the neutron midshell number. Interestingly, it is found that in our results the nucleus is normal deformed ($\beta_2 \geqslant 0.2$) when its $R_{4/2}$ ratio is above the shape transition point ($R_{4/2} = 0.3$). For ^{188,190}W, our calculated β_2 values are in agreement with those of FY+FRDM and ETFSI calculations, denoting prolate ground states, but in conflict with that of HFBCS calculation where their β_2 values are negative (corresponding to oblate shape). In addition, the β_4 deformations given by different theories show a consistent trend and sign for most of the nuclei,

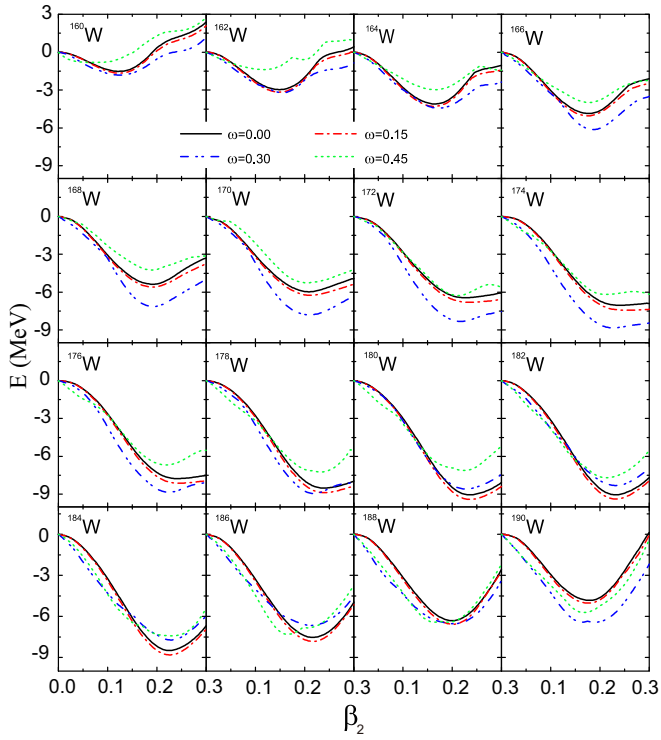

FIG. 2. Deformation Routhian curves against β_2 for even-even $^{160-190}$W nuclei at several selected rotational frequencies $\omega = 0.00$, 0.15, 0.30, and 0.45 MeV/$\hbar$. At each β_2 point, the energy was minimized with respect to γ and β_4.

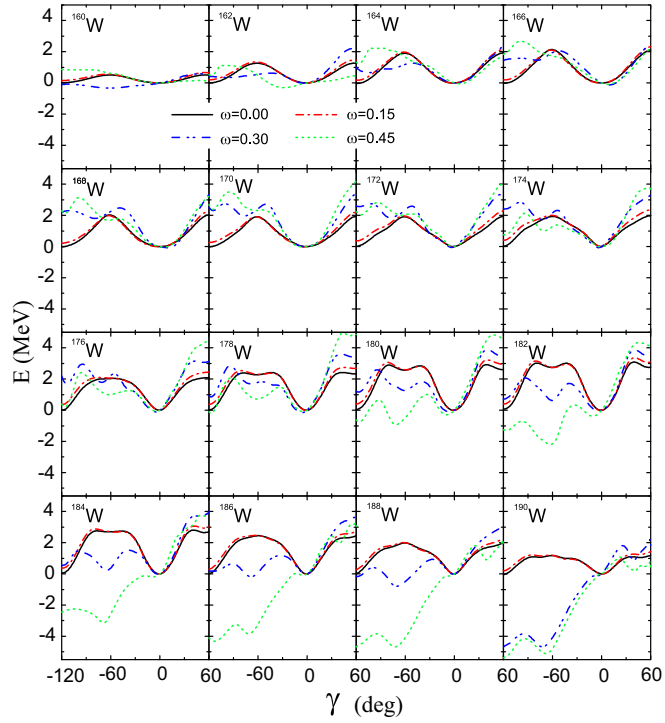

FIG. 3. Similar to Fig. 2 but against γ deformation.

in particular between present and FY+FRDM results, although their magnitudes are somewhat different.

As can be seen in Table I, the different theoretical results of the equilibrium deformations, which are determined by minimizing the calculated energy surface, may be somewhat different, especially for soft nuclei. Figures 2 and 3 show the corresponding total Routhian curves along the minimum valley of the TRS in both β_2 and γ directions, which are relatively model independent. The curves at four typical rotational frequencies are used to investigate the shape and softness evolutions under rotation. Because Bohr shape deformation parameters [37] are adopted in the actual calculations, the β_2 value is always positive and the prolate, oblate, and triaxial shapes can be denoted by the γ parameter. In rotating nuclei, we use the Lund convention [23] of γ values ranging from -120° to 60°. Such γ range can be divided into three sectors, $-120^\circ < \gamma < -60^\circ$, $-60^\circ < \gamma < 0^\circ$, and $0^\circ < \gamma < 60^\circ$, which represent the same triaxial shapes at ground state but, respectively, represent rotation about the long, intermediate, and short axes at nonzero cranking frequency. The four limiting values (-120°, -60°, 0°, and 60°) correspond to the possible rotations of axially symmetric shapes (-120° and 0° for prolate and $\pm 60^\circ$ for oblate shapes) with various orientations of the nuclear axes with respect to the rotation axis ($\gamma = -120^\circ$ and 60° mean the nucleus rotates around its symmetry axis, noncollective rotation, and $\gamma = -60^\circ$ and 0° mean the nucleus rotates around an axis perpendicular to the symmetry axis, collective rotation). As shown in Figs. 2 and 3, one can visually see the Coriolis effect as well as the evolution of nuclear shape and softness. For instance, the lighter nuclei ^{160,162}W are weakly deformed and have larger softness, especially in the γ direction. This is consistent with the recent work [8]. It is also found that the shape is very soft in the direction of increasing β_2 in $^{172-176}$W, especially in ^{174}W, indicating the possible occurrences of superdeformed structures, in good agreement with the results given by Dong *et al.* [61]. For the stable $^{180-186}$W and the neutron-rich ^{188,190}W nuclei, the competition of the prolate and oblate collective excitations and noncollective single-particle excitations (broken-pair high-K excitations) may appear at high angular frequency because the Fermi surfaces for both protons and neutrons lie in the upper shell of high-j orbits, although their ground states all have prolate shapes. Such competitions are consistent with some previous calculations [62–65]. Moreover, the similar competitions are also found in other isotopes such as No [66] and Rf [67] isotopes.

The calculated and experimental kinematic moments of inertia and the calculated aligned angular momentum are shown in Figs. 4 and 5, respectively. Note that the kinematic moments of inertia are, respectively, calculated by $J^{(1)} = I_x/\omega$ and $J^{(1)} = \hbar^2(2I-1)/E_\gamma(I \to I-2)$ theoretically and experimentally. It seems that our calculations can reproduce the experimental backbending (or upbending) phenomena, although the backbending frequencies are underestimated after ^{166}W; in particular the backbending in moments of inertia was not observed experimentally at present spins in $^{184-190}$W. As shown in Fig. 5, the proton and neutron aligned angular momenta can be used to evaluate the rotation alignments of proton and/or neutron pairs. The present results show that the neutron rotation alignment is favored in $^{164-180}$W, while in

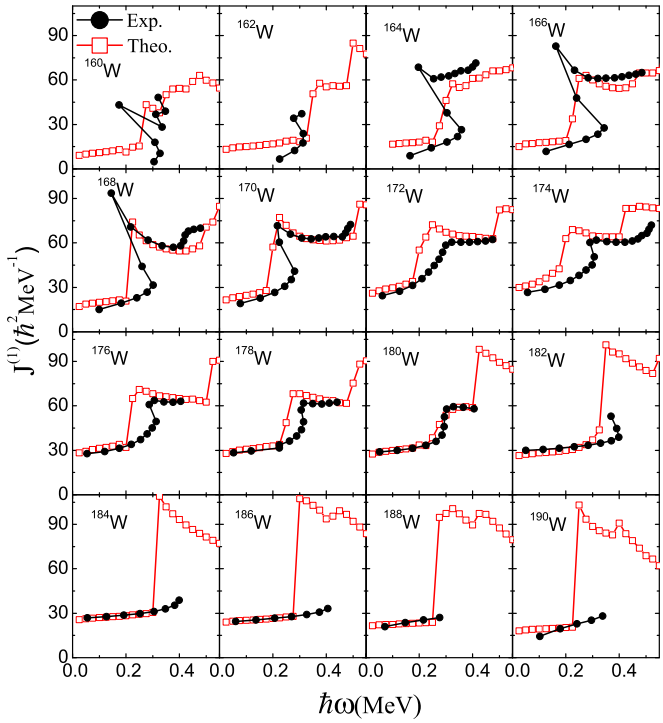

FIG. 4. The experimental (filled circle symbols) and calculated (open square symbols) kinematic moments of inertia $J^{(1)}$ for even-even nuclei $^{160-190}$W as a function of the rotational frequency $\hbar\omega$. The experimental data are taken from Ref. [41].

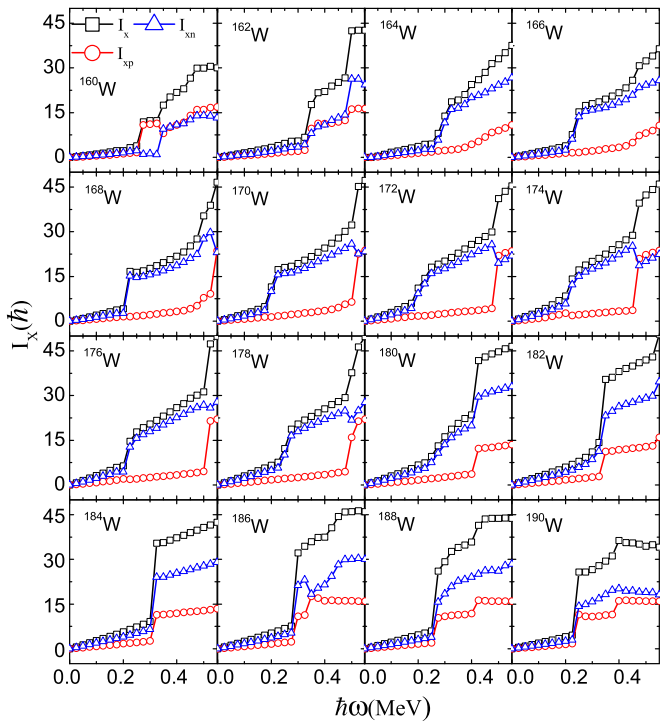

FIG. 5. The calculated aligned angular momenta I_x (squares), including the proton I_{xp} (circles) and neutron I_{xn} (triangles) components, for even-even nuclei $^{160-190}$W as a function of the rotational frequency $\hbar\omega$.

other nuclei the competition between the neutron and proton alignments may occur; even the proton alignment is favored in the very neutron-deficient nucleus ^{160}W. Of course, one can see that the magnitude of the neutron pair is larger than that of the proton pair in nuclei with alignment competitions except for ^{162}W. In this W isotopic chain, the high-j orbits associated with the rotation alignment mainly involve the proton $1h_{11/2}$ and neutron $2f_{7/2}$, $1h_{9/2}$, and $1i_{13/2}$ (the related discussions can be easily found elsewhere). It was pointed out by Xu *et al.* [18] that the adjustment of the pairing strength can improve the description in moments of inertia in this region. Indeed, our previous work showed both proton and neutron pairing correlations may be underestimated based on the present theory in this region [14]. Such an underestimation of the pairing correlation will be responsible for the reduction of the theoretical backbending frequency to a large extent. The degrees of the proton and neutron underestimations are usually different (cf. Ref. [14]), which indicates whether the proton and neutron rotation alignments still occur at the same frequency will need to be reconsidered then in those nuclei with competing proton and neutron alignments. This can be determined by the increased magnitude in moment of inertia, which should be larger when proton and neutron simultaneously align than that of only one alignment of them. However, as can be seen in Figs. 4 and 5, the increased magnitude in moment of inertia in $^{182-190}$W (proton and neutron alignments compete in them) cannot be experimentally extracted because of the scarce data. Fortunately, it seems that such a magnitude can be obtained crudely in ^{162}W. Actually, the increased magnitude in moment of inertia is less than that of the calculated result, indicating the possible occurrence of the rotation alignment of only one pair of nucleons. Of course, two neutron pairs may align at similar rotational frequencies. For instance, the two-quasineutron alignments emanating from the mixed $1f_{7/2}$ and $1h_{9/2}$ subshells can compete with the pure $1i_{13/2}$ two-quasineutron alignment in the very neutron-deficient W isotopes; see Ref. [8] and reference therein.

In addition, it is well known that the moment of inertia is sensitive to the pairing correlations. As shown in Fig. 6, we crudely investigate the effect of the pairing (including monopole and quadrupole pairing) correlations on the moment of inertia by taking three selected nuclei ^{164,172,180}W as examples. Note that the monopole pairing strength G_0 is crudely adjusted for protons and neutrons according to the empirical values of this mass region suggested by Xu *et al.* [18] (see Ref. [18] for more details about the pairing strength adjustment). From the comparison of Figs. 6(a) and 6(b), one can see that the increase of the monopole pairing strength to some extent decreases the moment of inertia and delays the backbending (or upbending) frequency, as expected, because of the increasing superfluidity and broken-pair difficulty, respectively. However, relative to the calculated results without the quadrupole pairing (QQ pairing) interaction, the existence of the QQ pairing force seems to increase the moment of inertia at the low-spin region but decrease the moment of inertia at high spins except for ^{172}W. From Fig. 6(b), it seems that the second band crossing in ^{172}W is attributed to the inclusion of the QQ pairing interaction. More detailed discussions of

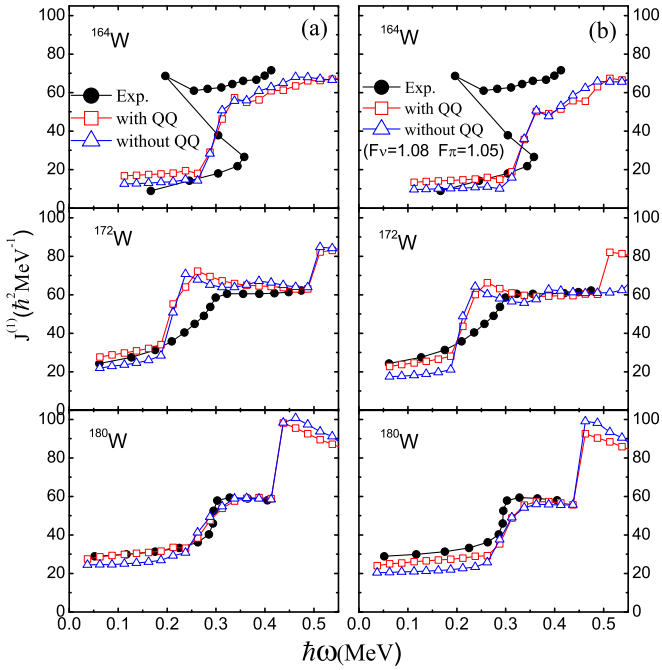

FIG. 6. Similar to Fig. 4, but for three selected nuclei ^{164,172,180}W. The open symbols (squares and triangles) denote the TRS results (with and without QQ-pairing interaction, respectively). The left (a) and right (b) panels show the calculated results with the pairing strengths obtained by the average gap method (G_0) and those adjusted, on average, for mean-field and blocking effects ($G = FG_0$), respectively. For reasons of simplicity, we use the constant factors $F_\nu = 1.08$ (neutrons) and $F_\pi = 1.05$ (protons) for the local mass region of the studied nuclei [18].

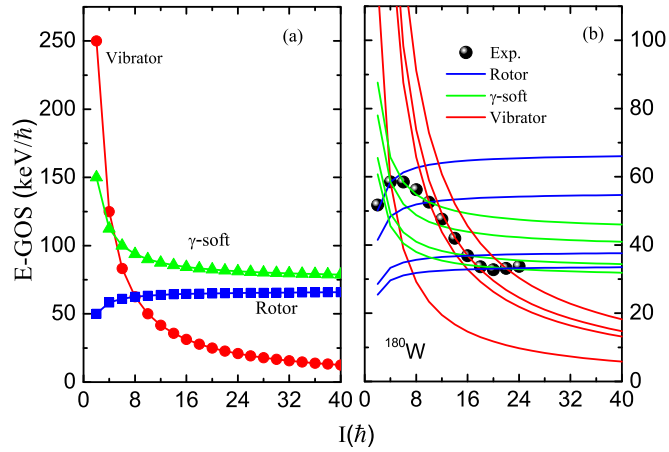

FIG. 7. (a) The typical E-GOS curves for a perfect harmonic vibrator, γ-soft, and axially symmetric rotors with first 2^+ excitations of 500, 300, and 100 keV, respectively [68]. (b) Similar to (a), four sets of such E-GOS curves at the selected spins $I = 4, 10, 16$, and $22\hbar$, together with the experimental data (filled circles) for ^{180}W. Note that at each selected spin point, the red, green, and blue lines denote the E-GOS curves with vibrational, γ-soft, and rotational modes, respectively.

the influence of the QQ pairing on nuclei can see, e.g., Refs. [31–34].

It can be noticed that there is a somewhat large difference in moment of inertia between theory and experiment even though the pairing strength is adjusted according to the experimental odd-even difference (e.g., see Fig. 6 and Ref. [18]). One has to think about other mechanisms by which atomic nuclei generate angular momentum, such as vibration and single-particle excitations. However, the present TRS approach, as a powerful tool in the analysis of yrast states, does not include the vibration mechanism which usually appears in excited state sequences. Indeed, the low-lying β and γ bands built on the so-called β vibrations with $K^\pi = 0^+$, and on the γ vibrations with $K^\pi = 2^+$, respectively, have been systematically observed in this mass region, e.g., in the W [42], Os [54], and Pt [56] isotopes. A simple empirical method, called E-GOS (E-Gamma Over Spin) curves [namely, the ratio $R(I) = \frac{E_\gamma(I\to I-2)}{I}$ versus I], was proposed by Regan *et al.* [68] for discerning the shape and phase evolution between vibrational and rotational structure in nuclei as a function of spin (moreover, the transitions not only from vibrational to rotational but also from rotational to vibrational motions have been found in different mass regions [68,69]). It is easy to understand that the γ-ray decay energies $E_\gamma(I \to I-2)$ can be given by $\hbar\omega$, $\frac{E(2^+)}{4}(I+2)$, and $\frac{\hbar^2}{2J}(4I-2)$, as given in Ref. [68], for a perfect harmonic vibrator, a γ-soft rotor, and an axially symmetric rotor, respectively. Correspondingly, the function relationships between $R(I)$ and I will be $\frac{\hbar\omega}{I}$, $\frac{E(2^+)}{4}(1+\frac{2}{I})$, and $\frac{\hbar^2}{2J}(4-\frac{2}{I})$. That is to say, the E-GOS curves can be plotted once the corresponding factors $\hbar\omega$, $\frac{E(2^+)}{4}$, and $\frac{\hbar^2}{2J}$ are determined, e.g., from the energy of the first 2^+ state. As shown by Regan *et al.* [68], the typical E-GOS plots are presented for the perfect harmonic vibrator, γ-soft rotor, and axially symmetric rotor with first 2^+ excitations of 500, 300, and 100 keV, respectively, in Fig. 7(a). In fact, one can deduce a set of $\hbar\omega$, $\frac{E(2^+)}{4}$ and $\frac{\hbar^2}{2J}$ factors from each $E_\gamma(I \to I-2)$ value by supposing it originates from the deexcitation of a pure vibrator, an idealized γ-soft rotor and an axially symmetric rotor, respectively. Therefore, based on each $E_\gamma(I \to I-2)$, we can plot three E-GOS curves passing through the corresponding $R(I)$ point. Moreover, if one of the assumptions is reasonable the adjacent point (except for the band crossing point) will generally fall on the corresponding curve. According to the existing data, Fig. 7(b) shows such E-GOS curves at several selected spins (including the low, medial, and high spins) for ^{180}W. It seems that the motion mode changes from rotation to γ-soft to vibration to rotation along the yrast line if the three idealized assumptions mentioned above are accepted.

In Fig. 8 we show such E-GOS curves at each spin point based on the available yrast data for even-even $^{160-190}$W. It should be noted that just for a clear display we keep the three corresponding curves from one $R(I)$ point to their next adjacent point $R(I+2)$. Thus, it seems that such a curve has many "legs" and let us call it as a centipedelike E-GOS temporarily. To a large extent, the structure evolution along the yrast line in even-even $^{160-190}$W can be evaluated from these centipedelike E-GOS curves, as shown in Fig. 8. One can see

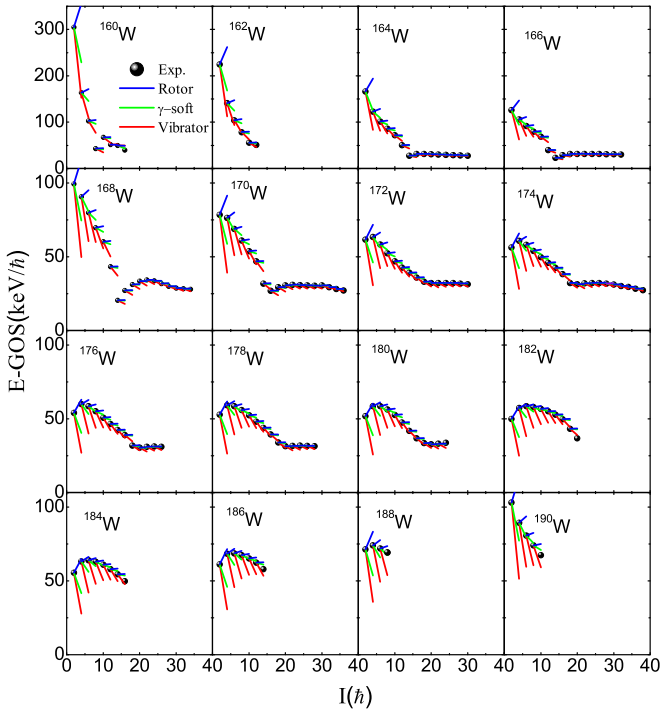

FIG. 8. Similar to the ^{180}W case of Fig. 7, but the centipedelike E-GOS curves along the yrast sequences for even-even $^{160-190}$W isotopes.

that the vibrational (or γ-soft) behaviors almost appear in all nuclei, even some of them (e.g, ^{162,190}W) have no rotational motions at present spins according to the centipedelike E-GOS picture. The absence of the vibration mechanism in the present TRS calculations may to some extent be responsible for the existing difference in moments of inertia between theory and experiment. In the lighter $^{160-168}$W nuclei, the nuclei may evolve from vibration (or γ-soft) to rotation while the phase transition from rotation to vibration (or γ-soft) occurs in the heavier nuclei $^{182-188}$W. Noted that the interesting transitions from rotation to vibration (or γ-soft) to rotation are found in $^{170-180}$W. Though the present TRS calculation does not consider the vibrational effect, some useful laws still can be found in the deformation energy curves, as shown in Figs. 2 and 3. Indeed, as expected, the minimum of the corresponding energy curve generally becomes soft when the transition from rotation to vibration occurs while it becomes stiff when the transition from vibration to rotation occurs. In addition, one can notice that the γ-soft and rotational E-GOS curves seem to coincide with each other at high spins. However, they can be qualitatively distinguished, in principle, because of the different signs of their curve slopes (negative and positive for the γ-soft and rotational cases, respectively). Of course, more precisely, the coupling of different motion modes should be considered, in particular, when the assumption of the purely single motion mode fails.

IV. SUMMARY

In summary, we have systematically investigated the collective nature along the yrast line for even-even $^{160-190}$W isotopes based on the pairing-deformation self-consistent TRS method in the (β_2,γ,β_4) deformation space. The calculated equilibrium deformations at ground states are compared with previous theoretical results and available experimental data, indicating a good agreement. The shape and softness evolutions under rotation are presented by using the deformation Routhian curves at different rotational frequencies. In addition, it is found that although the backbending phenomena in moments of inertia can be basically reproduced, the existing difference between experiment and theory is not eliminable, even if the pairing strength is adjusted accordingly. The properties of band crossings are analyzed briefly based on the calculated aligned angular momenta. The centipedelike E-GOS curves are introduced which show the shape and/or phase transition between vibration and rotation and provide an explanation for such discrepancy in moment of inertia to some extent, indicating the vibrational mechanism should be considered generally. This systematic investigation should be useful to understand and predict the yrast properties with rotation, in particular for the proton drip-line and neutron-rich nuclei where data are scarce.

ACKNOWLEDGMENTS

This work is supported by the Outstanding Young Talent Research Fund of Zhengzhou University (Grant No. 1521317002), the National Natural Science Foundation of China (Grants No. 11205207, No. 11205208, and No. 11505157) and the Foundation and Advanced Technology Research Program of Henan Province (Grant No. 132300410125).

[1] S. Frauendorf, Spontaneous symmetry breaking in rotating nuclei, Rev. Mod. Phys. **73**, 463 (2001).
[2] A. Bohr and B. R. Mottelson, *Nuclear Structure*, Vol. II (World Scientific, Singapore, 1998).
[3] M. J. A. de Voigt, J. Dudek, and Z. Szymański, High-spin phenomena in atomic nuclei, Rev. Mod. Phys. **55**, 949 (1983).
[4] A. Johnson, H. Ryde, and S. A. Hjorth, Nuclear moment of inertia at high rotational frequencies, Nucl. Phys. A **179**, 753 (1972).
[5] A. Fritsch, J. Q. Ginepro, M. Heim, A. Schuh, A. Shore, and M. Thoennessen, Discovery of the tungsten isotopes, At. Data Nucl. Data Tables **96**, 315 (2010).
[6] S. Goriely, M. Samyn, and J. M. Pearson, Further explorations of Skyrme-Hartree-Fock-Bogoliubov mass formulas. VII. Simultaneous fits to masses and fission barriers, Phys. Rev. C **75**, 064312 (2007).
[7] M. Thoennessen, Reaching the limits of nuclear stability, Rep. Prog. Phys. **67**, 1187 (2004).
[8] H. J. Li, B. Cederwall, T. Bäck, C. Qi, M. Doncel, U. Jakobsson, K. Auranen, S. Bönig, M. C. Drummond, T. Grahn, P. Greenlees, A. Herzáň, R. Julin, S. Juutinen, J. Konki, T. Kröll, M. Leino, C. McPeake, D. O'Donnell, R. D. Page, J. Pakarinen, J. Partanen, P. Peura, P. Rahkila, P. Ruotsalainen, M. Sandzelius, J. Sarén, B. Sayğı, C. Scholey, J. Sorri, S. Stolze, M. J. Taylor,

A. Thornthwaite, J. Uusitalo, and Z. G. Xiao, Recoil-decay tagging spectroscopy of $^{162}_{74}W_{88}$, Phys. Rev. C **92**, 014326 (2015).
[9] M. Bender, P. H. Heenen, and P. G. Reinhard, Self-consistent mean-field models for nuclear structure, Rev. Mod. Phys. **75**, 121 (2003).
[10] N. Wang, M. Liu, X. Z. Wu, and J. Meng, Surface diffuseness correction in global mass formula, Phys. Lett. B **734**, 215 (2014).
[11] D. R. Inglis, Particle derivation of nuclear rotation properties associated with a surface wave, Phys. Rev. **96**, 1059 (1954).
[12] D. R. Inglis, Nuclear moments of inertia due to nucleon motion in a rotating well, Phys. Rev. **103**, 1786 (1956).
[13] H. L. Wang, J. Yang, M. L. Liu, and F. R. Xu, Evolution of ground-state quadrupole and octupole stiffnesses in even-even barium isotopes, Phys. Rev. C **92**, 024303 (2015).
[14] H.-L. Wang, S. Zhang, M.-L. Liu, and F.-R. Xu, Nuclear stiffness evolutions against axial and non-axial quadrupole deformations in even-A osmium isotopes, Prog. Theor. Exp. Phys. 073D03 (2015).
[15] W. Nazarewicz, G. Leander, and J. Dudek, Octupole shapes and shape changes at high spins in Ra and Th nuclei, Nucl. Phys. A **467**, 437 (1987).
[16] W. Satuła, R. Wyss, and P. Magierski, The Lipkin-Nogami formalism for the cranked mean field, Nucl. Phys. A **578**, 45 (1994).
[17] W. Satula and R. Wyss, Coherence of nucleonic motion in superdeformed nuclei: Towards an understanding of identical bands, Phys. Rev. C **50**, 2888 (1994).
[18] F. R. Xu, R. Wyss, and P. M. Walker, Mean-field and blocking effects on odd-even mass differences and rotational motion of nuclei, Phys. Rev. C **60**, 051301 (1999).
[19] V. M. Strutinsky, Shell effects in nuclear masses and deformation energies, Nucl. Phys. A **95**, 420 (1967).
[20] R. Bengtsson, S. E. Larsson, G. Leander, P. Möller, S. G. Nilsson, S. Åberg, and Z. Szymański, Yrast bands and high-spin potential-energy surfaces, Phys. Lett. B **57**, 301 (1975).
[21] K. Neergård and V. V. Pashkevich, Shell corrections to the deformation energies of very high spin nuclei ($I \leqslant 100$), Phys. Lett. B **59**, 218 (1975).
[22] K. Neergård, V. V. Pashkevich, and S. Frauendorf, Shell energies of rapidly rotating nuclei, Nucl. Phys. A **262**, 61 (1976).
[23] G. Andersson, S. E. Larsson, G. Leander, P. Möller, S. G. Nilsson, I. Ragnarsson S. Åberg, R. Bengtsson, J. Dudek, B. Nerlo-Pomorska, K. Pomorski, and Z. Szymański, Nuclear shell structure at very high angular momentum, Nucl. Phys. A **268**, 205 (1976).
[24] W. Nazarewicz, R. Wyss, and A. Johnsson, Structure of superdeformed bands in the $A \approx 150$ mass region, Nucl. Phys. A **503**, 285 (1989).
[25] J. Dudek, B. Herskind, W. Nazarewicz, Z. Szymanski, and T. R. Werner, Pairing, temperature, and deformed-shell effects on the properties of superdeformed ^{152}Dy nucleus, Phys. Rev. C **38**, 940 (1988).
[26] W. D. Myers and W. J. Swiatecki, Nuclear masses and deformations, Nucl. Phys. **81**, 1 (1966).
[27] S. Cwiok, J. Dudek, W. Nazarewicz, J. Skalski, and T. Werner, Single-particle energies, wave functions, quadrupole moments and g-factions in an axially deformed Woods-Saxon potential with applications to the tow-center-type nuclear problems, Comp. Phys. Comm. **46**, 379 (1987).
[28] H. C. Pradhan, Y. Nogami, and J. Law, Study of approximations in the nuclear pairing-force problem, Nucl. Phys. A **201**, 357 (1973).
[29] P. Möller and J. R. Nix, Nuclear pairing models, Nucl. Phys. A **536**, 20 (1992).
[30] H. Sakamoto and T. Kishimoto, Origin of the multipole pairing interactions, Phys. Lett. B **245**, 321 (1990).
[31] M. Wakai and A. Faessler, Influence of quadrupole pairing on backbending, Nucl. Phys. A **295**, 86 (1978).
[32] M. Diebel, Influence of quadrupole pairing on rotational band-head energies, moments of inertia and band-crossing frequencies, Nucl. Phys. A **419**, 221 (1984).
[33] W. Satula and R. Wyss, Extended mean field description of deformed states in neutron deficient Cd-and Sn-nuclei, Phys. Scr. **T56**, 159 (1995).
[34] F. R. Xu, W. Satuła, and R. Wyss, Quadrupole pairing interaction and signature inversion, Nucl. Phys. A **669**, 119 (2000).
[35] J. Dudek, W. Nazarewicz, and T. Werner, Discussion of the improved parametrisation of the Woods-Saxon potential for deformed nuclei, Nucl. Phys. A **341**, 253 (1980).
[36] W. Greiner and J. A. Maruhn, *Nuclear Models* (Springer-Verlag, Berlin/Heidelberg, 1996).
[37] A. Bohr, Quadrupole degree of freedom for the nuclear shape, Mat. Fys. Medd. K. Dan. Vidensk. Selsk. **26**, 1 (1952).
[38] G. A. Leander, J. Dudek, W. Nazarewicz, J. R. Nix, and P. Quentin, Single-particle levels in the doubly magic ^{132}Sn and ^{100}Sn nuclei, Phys. Rev. C **30**, 416 (1984).
[39] P. Möller, J. R. Nix, W. D. Myers, and W. J. Swiatecki, Nuclear ground-state masses and deformations, At. Data Nucl. Data Tables **59**, 185 (1995).
[40] P. Ring, R. Beck, and H. J. Mang, On the application of the Hartree-Fock-Bogolyubov-equations to a microscopic theory of nuclear rotations, Z. Phys. **231**, 10 (1970).
[41] http://www.nndc.bnl.gov/.
[42] T. Kibédi, G. D. Dracoulis, A. P. Byrne, and P. M. Davidson, Low-spin non-yrast states in light tungsten isotopes and the evolution of shape coexistence, Nucl. Phys. A **688**, 669 (2001).
[43] C. A. Mallmann, System of Levels in Even-Even Nuclear, Phys. Rev. Lett. **2**, 507 (1959).
[44] J. B. Gupt, New perspective in potation vibration interaction, Int. J. Mod. Phys. E **22**, 1350023 (2013).
[45] F. Iachello, Analytic Description of Critical Point Nuclei in a Spherical-Axially Deformed Shape Phase Transition, Phys. Rev. Lett. **87**, 052502 (2001).
[46] N. Fouladi, J. Fouladi, and H. Sabri, Investigation of low-lying energy spectra for deformed prolate nuclei via partial dynamical SU(3) symmetry, Eur. Phys. J. Plus **130**, 112 (2015).
[47] R. F. Casten, D. S. Brenner, and P. E. Haustein, Valence p-n Interactions and the Development of Collectivity in Heavy Nuclei, Phys. Rev. Lett. **58**, 658 (1987).
[48] R. F. Casten, Possible Unified Interpretation of Heavy Nuclei, Phys. Rev. Lett. **54**, 1991 (1985).
[49] R. F. Casten, N_pN_n Systematics in heavy nuclei, Nucl. Phys. A **443**, 1 (1985).
[50] R. F. Casten and N. V. Zamfir, The evolution of nuclear structure: the N_pN_n scheme and related correlations, J. Phys. G: Nucl. Part. Phys. **22**, 1521 (1996).
[51] H. Watanabe, K. Yamaguchi, A. Odahara, T. Sumikama, S. Nishimura, K. Yoshinaga, Z. Li, Y. Miyashita, K. Sato, L. Próchniak, H. Baba, J. S. Berryman, N. Blasi, A. Bracco, F. Camera, J. Chiba, P. Doornenbal, S. Go, T. Hashimoto,

S. Hayakawa, C. Hinke, N. Hinohara, E. Ideguchi, T. Isobe, Y. Ito, D. G. Jenkins, Y. Kawada, N. Kobayashi, Y. Kondo, R. Krücken, S. Kubono, G. Lorusso, T. Nakano, T. Nakatsukasa, M. Kurata-Nishimura, H. J. Ong, S. Ota, Zs. Podolyák, H. Sakurai, H. Scheit, K. Steiger, D. Steppenbeck, K. Sugimoto, K. Tajiri, S. Takano, A. Takashima, T. Teranishi, Y. Wakabayashi, P. M. Walker, O. Wieland, and H. Yamaguchi, Development of axial asymmetry in the neutron-rich nucleus ^{110}Mo, Phys. Lett. B **704**, 270 (2011).

[52] A. S. Davydov and G. F. Filippov, Rotational states in even atomic nuclei, Nucl. Phys. **8**, 237 (1958).

[53] L. Wilets and M. Jean, Surface oscillations in even-even nuclei, Phys. Rev. **102**, 788 (1956).

[54] T. Kibédi, G. D. Dracoulis, A. P. Byrne, and P. M. Davidson, Low-spin non-yrast states and collective excitations in ^{174}Os, ^{176}Os, ^{178}Os, ^{180}Os, ^{182}Os and ^{184}Os, Nucl. Phys. A **567**, 183 (1994).

[55] P. M. Davidson, G. D. Dracoulis, T. Kibédi, A. P. Byrne, S. S. Anderssen, A. M. Baxter, B. Fabricius, G. J. Lane, and A. E. Stuchbery, Non-yrast states and shape co-existence in ^{172}Os, Nucl. Phys. A **568**, 90 (1994).

[56] P. M. Davidson, G. D. Dracoulis, T. Kibédi, A. P. Byrne, S. S. Anderssen, A. M. Baxter, B. Fabricius, G. J. Lane, and A. E. Stuchbery, Non-yrast states and shape co-existence in light Pt isotopes, Nucl. Phys. A **657**, 219 (1999).

[57] S. Raman, C. W. Nestor Jr., and P. Tikkanen, Transition probability from the ground to the first-excited 2^+ state of even-even nuclides, At. Data Nucl. Data Tables **78**, 1 (2001).

[58] S. Goriely, F. Tondeur, and J. M. Pearson, A Hartree-Fock nuclear masss table, At. Data Nucl. Data Tables **77**, 311 (2001).

[59] Y. Aboussir, J. M. Pearson, A. K. Dutta, and F. Tondeur, Nuclear mass formula via an approximation to the Hartree-Fock method, At. Data Nucl. Data Tables **61**, 127 (1995).

[60] J. Dudek, W. Nazarewicz, and P. Olanders, On the shape consistency in the deformed shell-model approach, Nucl. Phys. A **420**, 285 (1984).

[61] Y. S. Dong, S. Y. Yu, C. W. Shen, and Y. X. Liu, Possible existence of triaxial superdeformation in ^{172,174,176}W, Chin. Phys. C **33**, 103 (2009).

[62] C. F. Jiao, Y. Shi, F. R. Xu, Y. Sun, and P. M. Walker, Competition between collective oblate rotation and non-collective prolate K isomerism in neutron-rich tungsten isotopes, Sci. China-Phys. Mech. Astron. **55**, 1613 (2012).

[63] P. M. Walker and F. R. Xu, Prediction and possible observation of an oblate shape isomer in ^{190}W, Phys. Lett. B **635**, 286 (2006).

[64] P. D. Stevenson, M. P. Brine, Zs. Podolyak, P. H. Regan, P. M. Walker, and J. Rikovska, Shape evolution in the neutron-rich tungsten region, Phys. Rev. C **72**, 047303 (2005).

[65] K. Nomura, T. Otsuka, R. Rodríguez-Guzmán, L. M. Robledo, and P. Sarriguren, Structural evolution in Pt isotopes with the interacting boson model Hamiltonian derived from the Gogny energy density functiona, Phys. Rev. C **83**, 054303 (2011).

[66] F. Al-Khudair, G. L. Long, and Y. Sun, Competition in rotation-alignment between high-j neutrons and protons in transfermium nuclei, Phys. Rev. C **79**, 034320 (2009).

[67] H. L. Wang, Q. Z. Chai, J. G. Jiang, and M. L. Liu, Rotational properties in even-even superheavy $^{254-258}$Rf nuclei based on total-Routhian-surface calculations, Chin. Phys. C **38**, 074101 (2014).

[68] P. H. Regan, C. W. Beausang, N. V. Zamfir, R. F. Casten, Jing-ye Zhang, A. D. Yamamoto, M. A. Caprio, G. Gürdal, A. A. Hecht, C. Hutter, R. Krücken, S. D. Langdown, D. A. Meyer, and J. J. Ressler, Signature for Vibrational to Rotational Evolution Along the Yrast Line, Phys. Rev. Lett. **90**, 152502 (2003).

[69] S. F. Shen, Y. B. Chen, F. R. Xu, S. J. Zheng, B. Tang, and T. D. Wen, Signature for rotational to vibrational evolution along the yrast line, Phys. Rev. C **75**, 047304 (2007).